

# Millisecond dips in the RXTE/PCA light curve of Sco X-1 and TNO occultation

Hsiang-Kuang Chang<sup>1,2\*</sup>, Jau-Shian Liang<sup>1</sup>, Chih-Yuan Liu<sup>2</sup>, and Sun-Kun King<sup>3</sup>

<sup>1</sup>*Department of Physics, National Tsing Hua University, Hsinchu 30013, Taiwan*

<sup>2</sup>*Institute of Astronomy, National Tsing Hua University, Hsinchu 30013, Taiwan*

<sup>3</sup>*Institute of Astronomy and Astrophysics, Academia Sinica, Taipei 10617, Taiwan*

Accepted 2007 Month date. Received 2007 Month date; in original form 2007 Month date

## ABSTRACT

Millisecond dips in the RXTE/PCA light curve of Sco X-1 were reported recently (Chang et al. 2006), which were interpreted as the occultation of X-rays from Sco X-1 caused by Trans-Neptunian Objects (TNO) of hundred-meter size. Inconclusive signatures of possible instrumental effects in many of these dip events related to high-energy cosmic rays were later found (Jones et al. 2006) and the TNO interpretation became shaky. Here we report more detailed analysis aiming at distinguishing true occultation events from those related to cosmic rays. Based on some indicative criteria derived from housekeeping data and two-channel spectral information, we suggest that about 10% of the dips are probable events of occultation. The total number of TNOs of size from 60 m to 100 m is estimated to be about  $10^{15}$  accordingly. Limited by the coarser time resolution of standard data modes of RXTE/PCA, however, definite results cannot be obtained. Adequately configured observations with RXTE or other new instruments in the future are very much desired.

**Key words:** occultations – Kuiper Belt – Solar system: formation – stars: neutron – X-rays: binaries.

## 1 INTRODUCTION

The outer solar system beyond the orbit of Neptune is a relatively unfamiliar world to the human being, and yet it is believed to contain debris of the primordial solar disk and therefore carries much information about the early solar system. Although the existence of objects in the outer solar system was proposed long time ago (Leonard 1930; Edgeworth 1943, 1949; Oort 1950; Kuiper 1951), except for Pluto discovered by C. W. Tombaugh in 1930, the first of such objects was not found until 1992 (Jewitt & Luu 1993). Since then several surveys have been performed and about 1000 TNOs have been discovered (<http://cfa-www.harvard.edu/cfa/ps/lists/TNOs.html>).

The differential size distribution of the observed TNOs, which are all larger than about 100 km in diameter, follows a power law like  $dN/ds \propto s^{-q}$  with  $q = 4.0 \pm 0.5$  (e.g. Trujillo, Jewitt & Luu (2001); Luu & Jewitt (2002)). The size distribution, in addition to representing a major population property of TNOs, provides important constraints on the theory of how our planetary system was formed. In coagulation models of planet formation with collisional disruption cascade, for example, the power-law size

distribution does not simply extend towards smaller size but turns flatter (a smaller  $q$ ) below a certain break radius (e.g. Farinella, Davis & Stern (2000); Kenyon (2002); Kenyon & Bromley (2004)). The magnitude of the break radius depends on the initial mass in the trans-Neptunian region, the epoch of Neptune's formation, and the tensile strength of these small bodies. Extending our knowledge of the size distribution to smaller TNOs is clearly desirable.

TNOs smaller than 100 km are too dim to detect. A Hubble Space Telescope survey reported the detections of 3 TNOs within 0.02 square degrees of the sky, whose estimated diameters are about 30 km (Bernstein et al. 2004). These detections were achieved by blindly integrating images repeatedly over all possible TNO orbits for a total exposure of 22 ks. These 3 detections are a factor of 25 less than that expected from the extrapolation of the size distribution of TNOs larger than 100 km. For even smaller TNOs, occultation of background stars as a way to study their properties was proposed thirty years ago (Bailey 1976; Brown & Webster 1997; Cooray & Farmer 2003; Alcock et al. 2003; Roques et al. 2003). Searches for such occultation events in optical bands have been conducted by many groups but without any definite detection so far. Three possible detections were just reported recently (Roques et al. 2006).

\* E-mail: hkchang@phys.nthu.edu.tw

On the other hand, occultation events in X-rays may stand a better chance of detection, compared with the optical band. The photon-counting nature of X-ray detectors like proportional counters provides much faster photometry and the much shorter wave length of X-rays means much less diffraction. These two features make it more feasible to detect events caused by smaller bodies, and henceforth can provide a larger number of possible events. This technique requires a bright background X-ray source. Sco X-1, the brightest X-ray source in the sky, serves this purpose well. Its location, only about 5.5 degrees north of the ecliptic, allows good sampling of the TNO population. The Proportional Counter Array (PCA) on board Rossi X-ray Timing Explorer (RXTE) (Bradt, Rothschild & Swank 1993), a NASA satellite, has the largest effective area in the keV X-ray band. The typical RXTE/PCA count rate of Sco X-1 is  $10^5$  counts per second. It is therefore possible to search for occultation events at millisecond time scales.

Millisecond dip events in the X-ray light curve of Sco X-1, in total 58 in 322-ks data, were reported recently (Chang et al. 2006), which were attributed to occultation caused by small TNOs. Later, signatures of possible instrumental effects related to high energy cosmic rays for many of these dip events were found (Jones et al. 2006) and their nature became uncertain. In this paper, we report further analysis of 107 dip events (including the original 58), which were found in 564-ks RXTE archival data spanning over 7 years from 1996 to 2002. The procedure to identify these events and their properties are described in Section 2. Signatures of possible instrumental effects are discussed in Section 3. In Section 4 we propose some criteria to tentatively separate true astronomical events from those likely due to the instrumental dead-time effect. We then further argue that those dip events without indication of instrumental effects are occultation caused by small TNOs and derive the total number of TNOs in the corresponding size range in Section 5.

## 2 MILLISECOND DIPS IN THE RXTE/PCA LIGHT CURVE OF SCO X-1

To search for possible occultation events, we examined the light curves of Sco X-1 binned in different bin sizes from all the available RXTE/PCA archival data and computed their deviation distributions. The definition of the ‘deviation’ employed here can be found in Chang et al. (2006). The deviation distribution of all the time bins in the light curve should be of a Poisson nature modified by the dead-time and coincidence-event effects if all the fluctuations are random and there is no occultation event. One example of such a deviation distribution is shown in Fig. 1, in which the search was conducted with 2-ms time bins. The excess at the negative deviation end is obvious. We performed the search with different time-bin sizes ranging from 0.5 ms to 20 ms. In each search, those time bins with a negative deviation of random probability lower than  $10^{-3}$  were selected. It corresponds to a negative deviation of about  $7\sigma$  in the deviation distribution, depending on the total number of time bins in that search. In total, 107 dip events were identified in 564-ks data, many of which appear more than once in searches with different bin sizes. The epochs of all the 107 events are listed

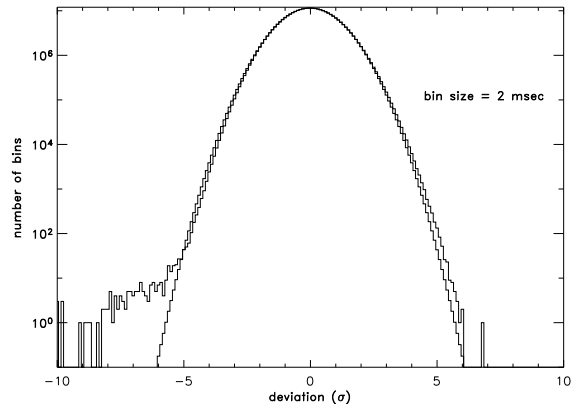


**Figure 1.** Example deviation distribution of the Sco X-1 RXTE/PCA light curve. See Chang et al. (2006) for the exact definition of the deviation. The thick histogram is from the 564-ks RXTE/PCA data of Sco X-1 and the thin one is a Gaussian distribution, plotted for comparison. To show the relatively small number of events with large deviations, the ordinate is plotted in logarithmic scales. The excess at the negative deviation end is obvious. The small excess at the positive deviation part and the tiny deficiency between about  $-3\sigma$  and  $-5\sigma$  are due to the Poisson nature of the observed photons.

in Table 1 for later referring and for readers’ convenience to find them in the RXTE data.

Some example light curves of these dip events are shown here in Fig. 2. These light curves show a variety of characteristics. About one half of all the events have a duration of 2 ms, and most of the rest are 1.5-ms and 2.5-ms events. The longest one is 7 ms. The flux-drop fraction of these events,  $A$ , defined as  $A = (1 - f)$  with  $f$  being the ratio of the average counts per bin within the event to that outside the event in a 100-ms window, is distributed between 0.3 and 0.8. Fig. 3 shows the distribution of the 107 events in duration and in the flux-drop fraction. The event duration is defined as the length of the time interval in which the photon count number in a 0.5-ms bin is smaller than one standard deviation below the average counts per 0.5-ms bin in a 100-ms window. This definition, instead of considering all the bins with photon counts just below the average, avoids a probably inadequate designation of a longer duration to cases like event 31 in Fig. 2 and event 5 in Fig. 12. However, a more complicated dip light curve may simply be missed with our definition, such as event 9 and 101 in Fig. 2. Adopting the average counts as the threshold to define the duration will include the trailing dip of event 9 but not event 101. To have an operational definition without arbitrary, subjective selection judgment, we adopt our current definition. This definition tends to somewhat underestimate the duration and overestimate the flux-drop fraction. We note that our detection method as described above is biased against events of a small flux-drop fraction. In the case of a search with time bins of 2 ms, for example, those time bins falling between  $-5\sigma$  and  $-7\sigma$  contain a mixture of random and good events and are not selected (see Fig. 1). This procedure is also biased against events much shorter than about 1 ms because of the small count number in one bin.

Many of the events have an asymmetric light curve with

**Table 1.** Epoch list of the 107 dip events.

event	epoch (MJD)	event	epoch (MJD)	event	epoch (MJD)	event	epoch (MJD)
1	50127.47287408	28	50560.64741831	55	50820.82725554	82	50999.28352289
2	50127.48015520	29	50560.74484861	56	50820.84952867	83	50999.35461803
3	50227.88200130	30	50560.79377724	57	50820.89743563	84	50999.41091596
4	50227.95654701	31	50560.80657724	58	50820.97524034	85	51184.53187584
5	50228.08619841	32	50561.59186087	59	50820.98661576	86	51186.48533043
6	50228.42335989	33	50561.59809735	60	50821.10690660	87	51186.62284120
7	50228.94854367	34	50561.60711487	61	50821.50189352	88	51187.09077119
8	50229.20952234	35	50561.60902924	62	50821.92314378	89	51187.81352256
9	50229.28446027	36	50562.67774632	63	50963.22196721	90	51187.95222912
10	50229.95584931	37	50562.73583564	64	50963.22696160	91	51188.00380963
11	50229.95809071	38	50664.04398279	65	50963.29032203	92	51188.01842742
12	50230.09181139	39	50682.18029159	66	50964.27470971	93	51188.02324544
13	50230.13947224	40	50816.96028303	67	50964.28074489	94	51188.35803894
14	50230.95055234	41	50816.96908550	68	50964.28618818	95	51188.61416433
15	50231.07426689	42	50817.04546707	69	50964.29270126	96	51191.87259403
16	50231.08555152	43	50817.04865761	70	50965.27044441	97	51191.87461469
17	50231.12912418	44	50817.90240868	71	50965.29753470	98	51191.87770321
18	50522.78695518	45	50818.05516266	72	50965.34610105	99	51191.93625665
19	50522.89848183	46	50818.77866986	73	50966.12939997	100	51192.94289686
20	50522.91066851	47	50818.77931186	74	50966.16083347	101	51193.80435748
21	50522.92443425	48	50819.10373772	75	50966.22742241	102	51194.87184245
22	50522.95734852	49	50819.62710164	76	50996.34615057	103	52348.09450448
23	50522.95752945	50	50819.98466883	77	50997.26933552	104	52409.88829219
24	50558.87343683	51	50820.11086494	78	50997.41920381	105	52410.89054165
25	50558.92531729	52	50820.62648648	79	50998.33941018	106	52410.95092608
26	50559.86445702	53	50820.70592722	80	50998.34211168	107	52413.98904378
27	50559.93855131	54	50820.71036958	81	50999.27356237		

fast drop and slow recovery, like event 21 and 84 shown in Fig. 2. To characterize the degree of asymmetry, we define the ‘skewness’,  $S$ , of each event as

$$S = \frac{1}{N} \sum_x C_x \left( \frac{x - \langle x \rangle}{\sigma} \right)^3, \quad (1)$$

where  $N$  is the total number of ‘missing photons’ within the event duration relative to the average count level of a 100-ms window,  $x$  is time and runs for each time bin,  $C_x$  is the number of missing photons in time bin  $x$ , and  $\sigma$  is the standard deviation of this missing-photon distribution in time ( $\sigma^2 = \sum_x C_x (x - \langle x \rangle)^2 / (N - 1)$  and  $\langle x \rangle = \sum_x x C_x / N$ ). With such a definition,  $N$  and  $C_x$  are in general not integers. The skewness is then normalized to  $\sqrt{15/N}$ , which is roughly equal to the standard deviation in skewness randomly drawn from a Gaussian distribution of  $N$  photons (Press et al. 1992). The skewness is zero for symmetric light curves and positive for light curves with fast drop and slow recovery. The skewness distribution of the 107 events is shown in Fig. 3. It appears that there seems to be two populations of events in terms of skewness.

### 3 SIGNATURES OF POSSIBLE INSTRUMENTAL EFFECTS

It was pointed out in Jones et al. (2006) that many of these dip events may be related to the so-called ‘very large event’ (VLE), in the RXTE terminology. Unfortunately, the VLE counts were recorded with a 125-ms resolution. Besides, not all the individual VLE bins covering the dip epochs have an

unusual high count number. The association of VLEs and dip events is so far not conclusive. Prompted by the report in Jones et al. (2006), we examined some more particle-related properties of these dips, in the hope to properly assess the instrumental signatures and to identify non-instrumental dip events, if the current data allows.

A VLE is an event that deposits more than about 100 keV energy in any one of the six active xenon-layer anodes or the propane-layer anode in each Proportional Counter Unit (PCU) of the PCA on board RXTE. Technical details of RXTE instrumentation can be found in the RXTE web site and also in Jahoda et al. (2006). A VLE saturates the preamplifier and causes ringing in the signal chain when the amplified signal is restored to the baseline. A larger dead-time window is set for each VLE. For most of the Sco X-1 observations it was chosen to be about 70  $\mu$ s (Jahoda et al. 2006). The actual duration in which the signal chains are affected depends on the pulse height of the saturating event. The VLE counts are recorded with a 125-ms time resolution in the ‘standard-1’ data mode for every PCA observations. The standard-1 data mode also records, with the same 125-ms resolution, the propane-layer counts, which are events that trigger only the propane layer, and the ‘remaining’ counts, which are all the events except for ‘good’ events, VLEs, and propane events. Good events are those trigger only one xenon anode. The propane layer is designed to distinguish events caused by soft electrons from those by X-rays. The ‘remaining’ counts contain many ‘multiple-anode’ events, which are usually treated as particle background. Because Sco X-1 is very bright, most of the propane-layer events and the ‘remaining’ events are in fact caused by pho-

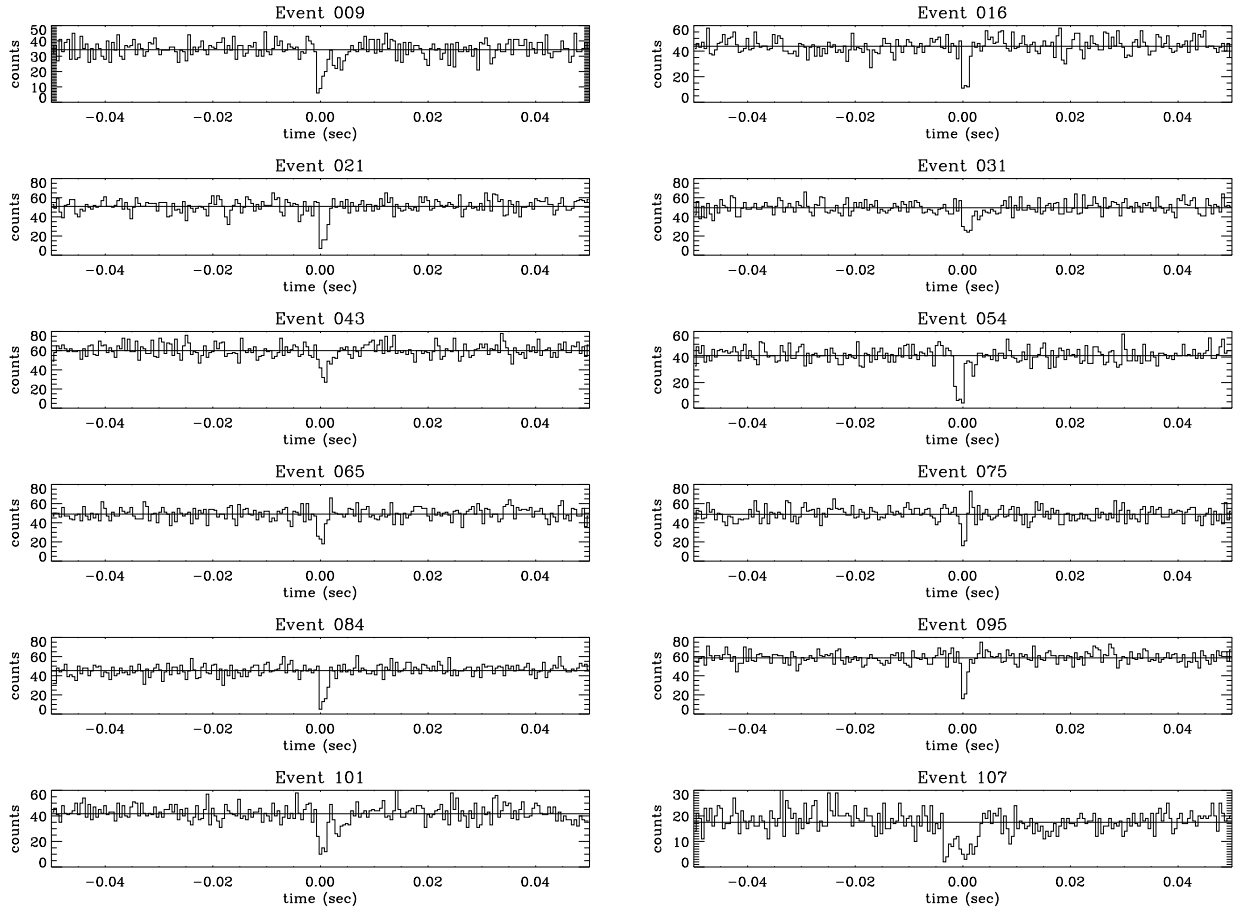


**Figure 2.** RXTE/PCA light curves of some example dip events. Horizontal lines are the average counts in each panel. The histograms are plotted with a bin size of 0.5-ms. events are numbered in sequence according to their occurrence epoch. Different count rates for different observations are due to the intrinsic flux variation of Sco X-1 and the number of PCUs turned on in that observation.

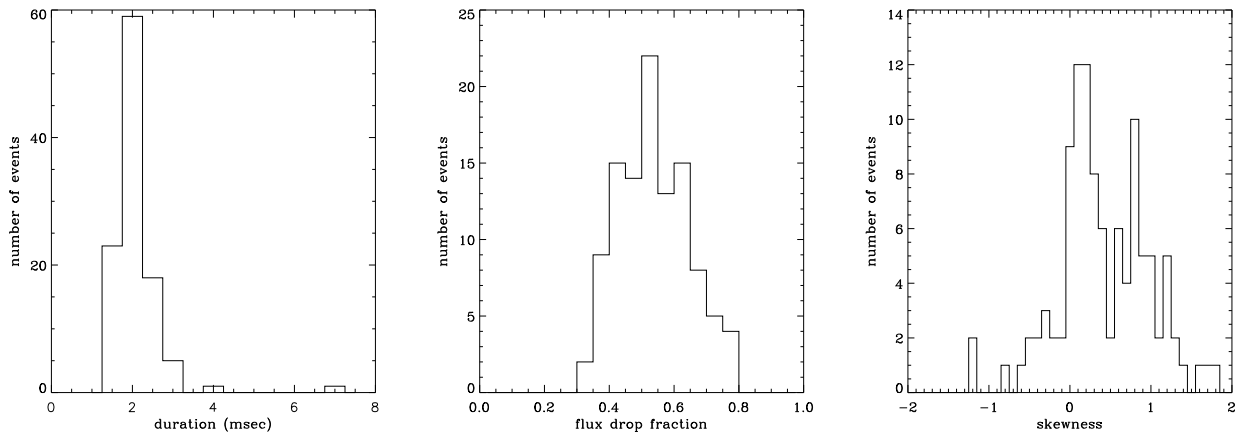


**Figure 3.** Distributions in the duration, flux drop fraction, and skewness of the 107 events.

tons from Sco X-1. In most of the Sco X-1 observations, the data mode recording events triggering both the ‘left’ and ‘right’ xenon anodes of the first layer (L1&R1) with a 250- $\mu$ s time resolution is also employed. Almost all of these L1&R1 coincidence events are caused by photons from Sco X-1, instead of particles. All the above information is useful

for investigating the possible instrumental effects for the dip events. Unfortunately the 125-ms resolution is much larger than the dip event duration. More detailed information is recorded in the ‘standard-2’ data mode but with an even coarser resolution of 16 s.

In Fig. 4, example light curves of good counts, L1&R1

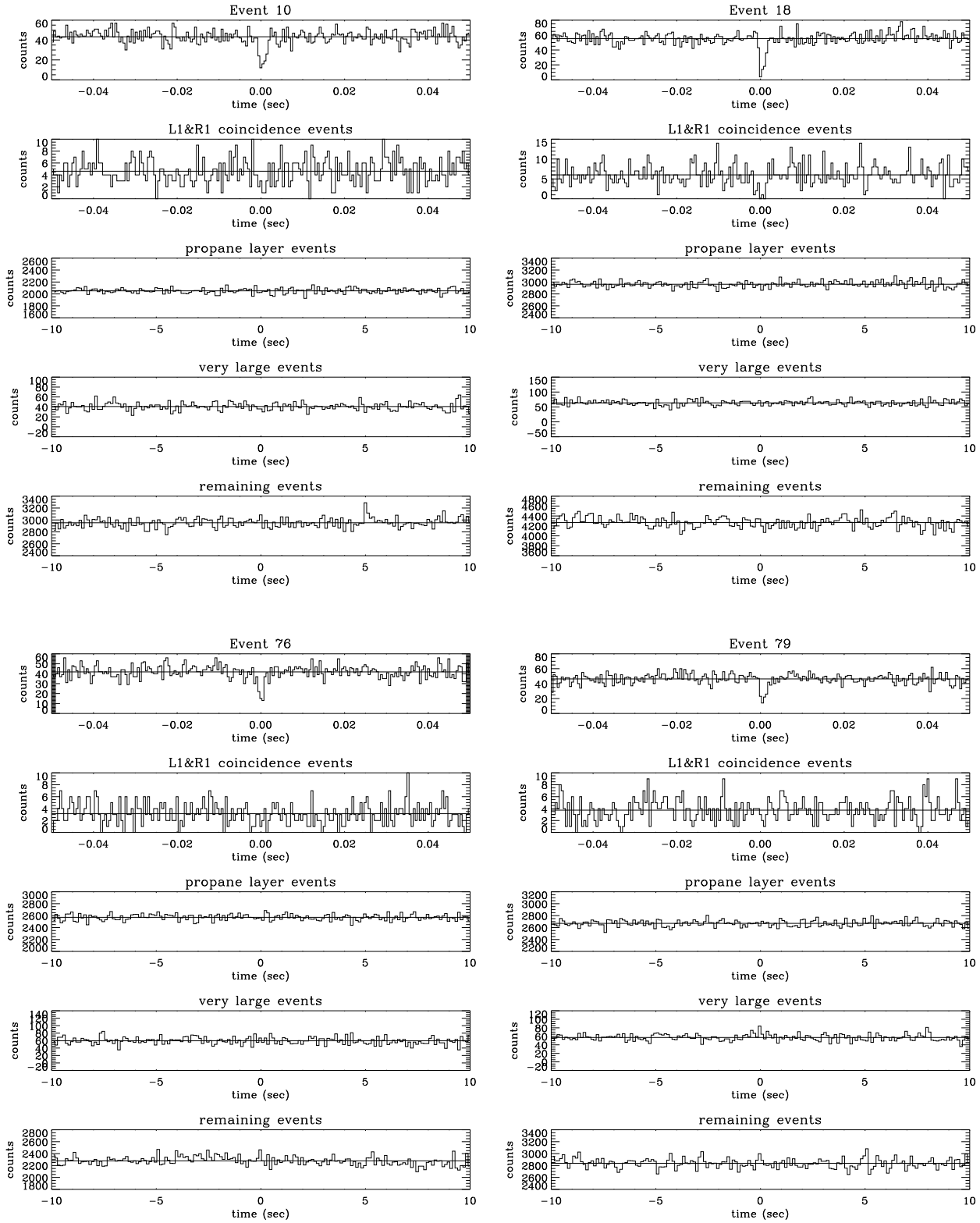


**Figure 4.** Example light curves of good counts, L1&R1 coincidence counts, propane-layer counts, VLE counts, and ‘remaining’ counts of 4 dip events. For each dip event, the time zero of all the 5 light curves is referred to the same epoch. Please note the different time scales in the abscissae. Each time bin in the light curve of good counts and L1&R1 counts is 0.5 ms. That in the other three is 125 ms. None of these 4 is selected as a probable non-instrumental event; see discussion in the text.

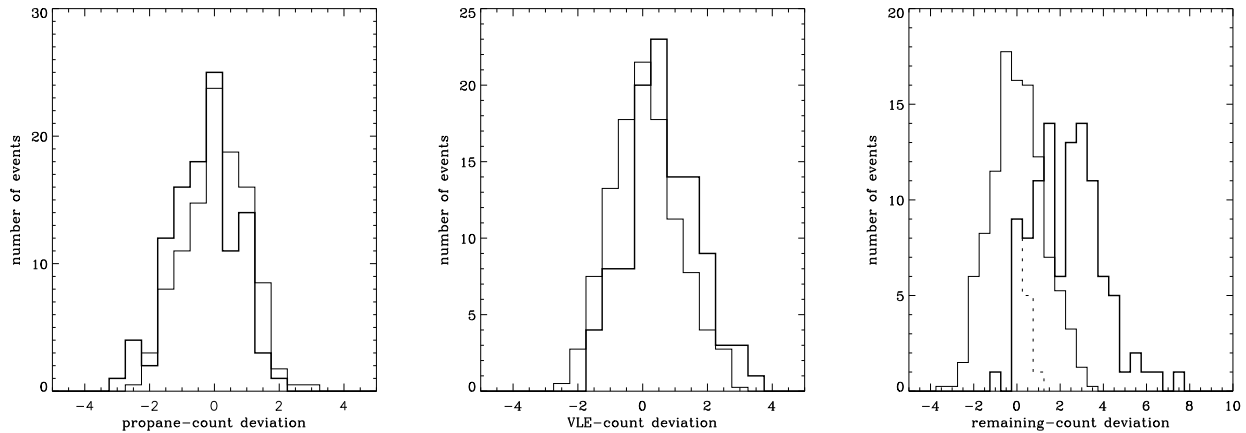


**Figure 5.** Deviation distributions of the propane counts, VLE counts and ‘remaining’ counts. Thick histograms are for the 107 dip events and thin ones are the average of 4 comparison groups. The dashed line in the right panel is explained in Section 4. The ‘remaining’ deviations of event 7, 101 and 107 are larger than 10 and are not included in the right panel.

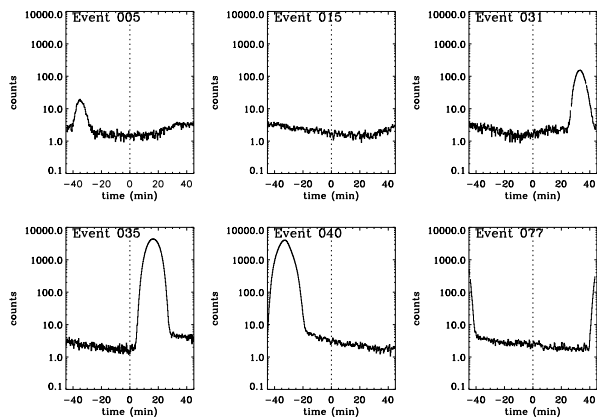


**Figure 6.** Some example light curves of HEXTE/PM counts. The vertical dashed lines indicate the dip event epochs. SAA passage is clearly seen in the HEXTE/PM counts. Many of the 107 dip events are far away from the SAA passage, like event 15 shown here. The time difference between the epochs of the dip and the nearest SAA peak passage is defined as the time since SAA.

coincidence events, propane-layer events, very large events, and ‘remaining’ events are shown. The time zero of all the 5 light curves is referred to the same epoch. For all the 107 events, the L1&R1 coincidence counts all drop consistently with the dip, although sometimes not so obviously because of the small count number. The propane-layer events in fact do not show any anomaly. Many of the 107 events are associated with higher VLE counts, like event 79 in Fig. 4. Their VLE counts are not unusually high. Only when all the events are studied together, the tendency of having a higher VLE count number becomes clear. We note that, however, a higher VLE count does not always come with a dip event. In Fig. 4, there are several VLE bins with a higher count number similar to that at the dip epoch of event 79. There are no dip events in those time bins. A clearer indication of possible instrumental effects appears in the ‘remaining’ counts. Almost all the 107 events are associated with a ‘re-

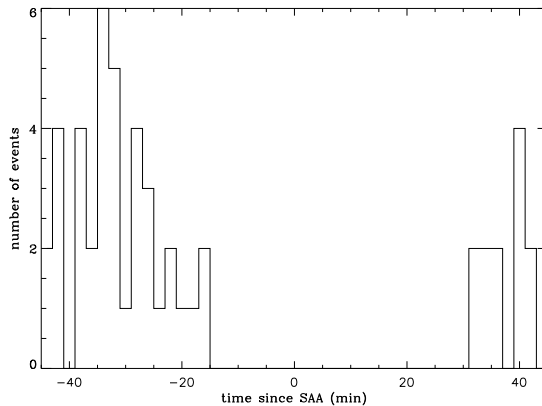


**Figure 7.** The distribution of dip events according to their ‘time since SAA’, defined in the caption of Fig. 6. The histogram bin size is 2 minutes. 50 out of the 107 dip events are within 45 minutes before and after the SAA peak passage and are all included in this figure. The gap around the SAA passage is because of data screening.

maining’ count number larger than the average in a local window.

To better present all these count excesses, we define, for each dip event, the propane deviation, VLE deviation, and ‘remaining’ deviation as the difference between the corresponding count number and the average in a certain window encompassing the bin in question. The deviation is then further expressed in units of the square root of that average. These deviation distributions are plotted in Fig. 5. The average ‘remaining’ count rate sometimes varies noticeably at time scales about 2 s or so. We therefore used a window containing 9 bins (about 1 s) for the computation of these deviations. A comparison deviation distribution is also shown together in Fig. 5. The comparison distribution is the average of four distributions drawn from the bin at -4s, -2s, +2s and +4s away from the bin covering the dip epoch respectively. This comparison distribution is a representation of the distribution without contamination from the suspected

particle events. One can see that there is nothing unusual in the propane-count deviation. The VLE deviation distribution exhibits a positive shift but still contains a considerable population of negative deviation. The ‘remaining’-count deviation distribution shows a very significant positive shift.

To further investigate the possible particle association, we computed the time difference between the dip epoch and the nearest SAA peak passage. It was done with the data obtained with the two particle monitors of the instrument HEXTE (Rothschild et al. 1998). Some examples are shown in Fig. 6. The event distribution in the time since SAA is shown in Fig. 7, in which all the dip events within 45 minutes before and after the SAA peak passage are included. One can see that there is no indication of any correlation between the dip epoch and the SAA passage. The suspected particle events are not related to the SAA. We have also examined other characteristics of these dip events and found no obvious correlations among the duration, flux-drop fraction, skewness, VLE deviation, ‘remaining’ deviation and time since SAA either. That the dip skewness is not related to the VLE or ‘remaining’ deviations is somewhat puzzling. The skewness versus those deviations and the time since SAA is plotted in Fig. 8.

68 dip events out of the 107 are in observations with a data mode carrying two-channel spectral information. The energy bands for these two channels are about 2-5 keV and 5-18 keV. There seems to be a trait that the flux drop fraction is higher in the high energy band than in the low energy one. Some examples are shown in Fig. 9. The distribution of the ratio of the flux-drop fraction in the high energy band to that in the low energy one for each dip events is plotted in Fig. 10. Occultation events, because of diffraction, will have a smaller flux drop in a lower energy band, while the instrumental dead-time effect does not have that energy dependence. Although random fluctuation may render individual identification unreliable, Fig. 10 suggests that, statistically speaking, some dip events may not be caused by instrumental effects.

It was proposed in Jones et al. (2006) that ‘the dips are caused by electronic dead time in response to some type of charged particle shower in the spacecraft.’ Indeed, the positive deviation in the VLE and ‘remaining’ counts associated with dip events within 125-ms uncertainty (Fig. 5) indicates that, at least statistically speaking, many of the dip events are likely due to the dead-time effect caused by particles. To have such a large flux drop for such a long period, however, several PCUs must be affected at the same time and a very large amount of charged particles is needed. The PCA has 5 almost identical PCUs. The usual signal dead time is about  $10\mu\text{s}$ , and that for a VLE signal is about  $70\mu\text{s}$ . That the ‘remaining’ excess is much more significant than the VLE one indicates that the dead time caused by the hypothesized lower-energy secondary particles or by the VLE ringing events may be the major, direct cause for these dips. Although the Crab nebula is about 8 times dimmer than *Sco X-1* and therefore individual dips cannot be identified, an excess at the negative end of the deviation distribution may be expected if the data amount is enough. However, because the flux-drop fraction of these dips is not close to unity, but distributed between 0.3 and 0.8, they, at a rate of about one per 5 ks, are not noticeable in the deviation distribution drawn from the 380-ks RXTE/PCA archival data

of the Crab nebula. On the other hand, the indication so far is not strong enough to argue that all the dips are caused by the cosmic-ray induced dead-time effect. There are dip events whose associated ‘remaining’ and VLE deviations are negative or very small. There are time bins (125 ms) with large VLE or ‘remaining’ excesses but without any dips. Furthermore, the flux-drop fraction of the dip events is generally larger in the high-energy band than in the low-energy one, a signature of diffraction. It is likely that these dips are heavily contaminated by particle-related events, but not all of them are caused by the instrumental dead-time effect.

#### 4 EVENTS WITHOUT INDICATION OF INSTRUMENTAL EFFECTS

Limited by the 125-ms time resolution of the standard-1 data, it is impossible to definitely identify individual dip events as caused by the instrumental dead-time effect or as of a probable astronomical origin. Nevertheless, as discussed in the previous section, it is likely that these dip events are a mixture of the two kinds. Since the light-curve skewness and the ‘time since SAA’ are not correlated with the VLE or ‘remaining’ deviations, we propose to select those probable non-instrumental dip events solely based on the two deviations. From Fig. 5, one can see that the comparison population has a half width at half maximum of about 1.25 in both deviation distributions. If a non-instrumental population exists, the half width in the deviation distribution is about the same. In this regard, a somewhat conservative criterion to identify probable non-instrumental events can be set as the VLE and ‘remaining’ deviations being both smaller than 1.25.

From the ‘remaining’ deviation distribution in Fig. 5, the total number of the probable non-instrumental events can be estimated by assuming all the events with a negative ‘remaining’ deviation are the probable non-instrumental events and they have a more or less symmetric deviation distribution centered at zero deviation. Such a possible distribution is plotted in dashed lines in Fig. 5. The total number estimated this way is about 16. This number is of course somewhat arbitrary and only suggestive. The sum of the two deviations can be taken as a measure and the second criterion can be set, to be conservative again, as that sum being smaller than 1.0 so that the total number is 12. These two criteria are also shown in Fig. 11. The light curves of the 12 probable non-instrumental events are shown in Fig. 12.

The second criterion is somewhat arbitrary. We have conducted such a selection procedure with different window size for computing the ‘remaining’ deviation. 8 dip events among the 12 are always selected even when the window is as large as 10 s. The 4 left out (event 41, 52, 59, and 74) are all those with the ‘remaining’ count level varying at 2-s time scales. We think the 1-s window, which we employed to compute the ‘remaining’ deviation distribution shown in Fig. 5, is a more meaningful one and therefore adopt the 12 dip events selected with the procedure mentioned above as the probable non-instrumental events. Among the 12 probable events, 7 (event 19, 41, 52, 59, 61, 66, and 74) have two-channel spectral information. Their flux-drop-fraction ratios of high- to low-energy bands are all larger than unity.

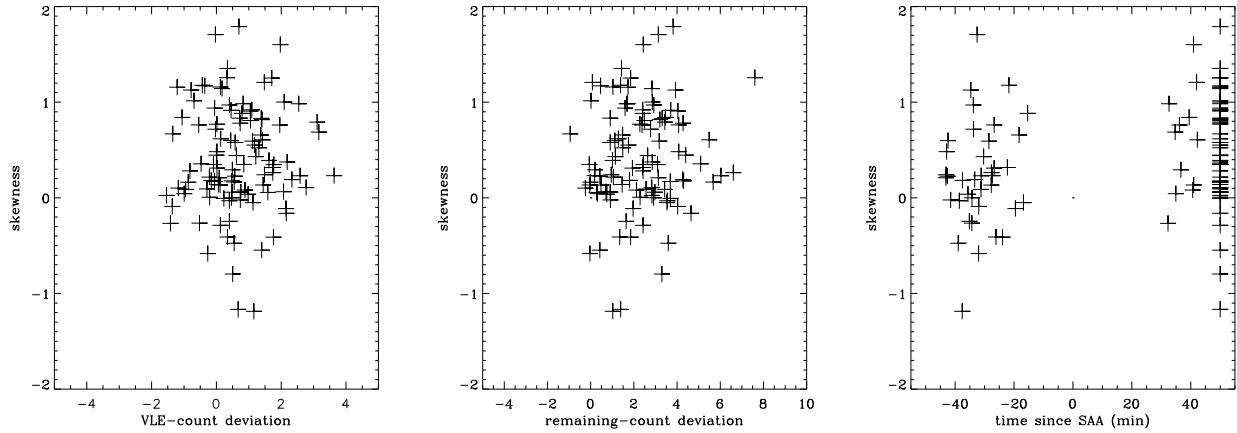


**Figure 8.** The VLE deviation, ‘remaining’ deviation and time since SAA versus the dip skewness. Event 7, 101 and 107, with a ‘remaining’ deviation larger than 10, are not included in the central panel. In the right panel, all the dips outside the  $\pm 45$ -min window of an SAA peak passage are plotted at the time since SAA equal to 50 min.

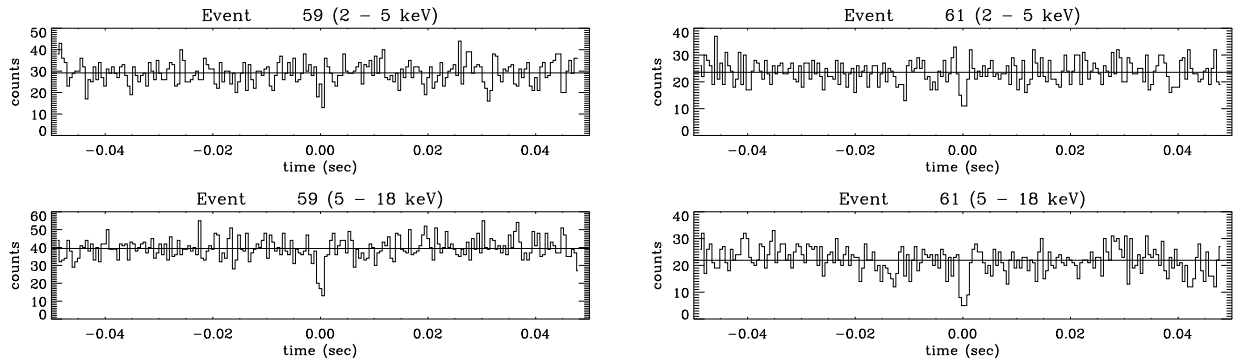


**Figure 9.** The light curves of event 59 and 61 in two energy bands.

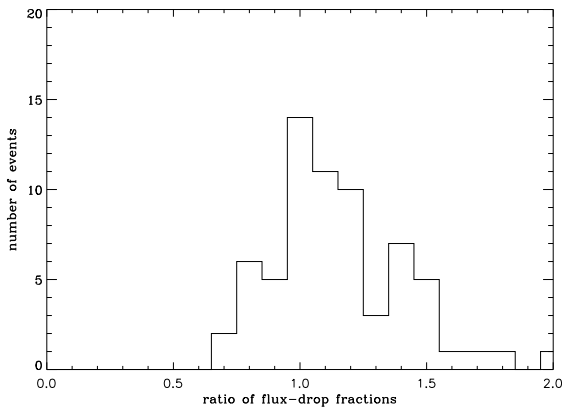


**Figure 10.** Distribution of the flux-drop fraction ratio. The ratio is the flux-drop fraction in the high-energy band (5-18 keV) divided by that in the low-energy one (2-5 keV).

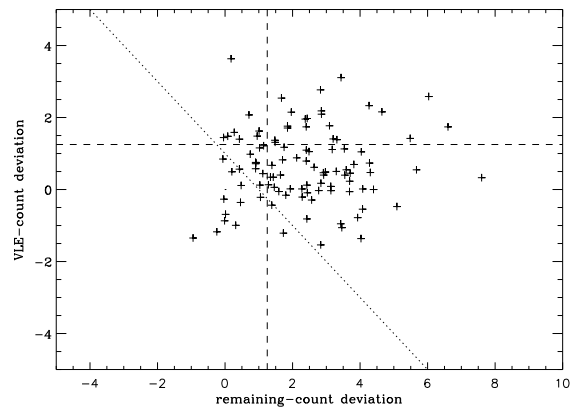


**Figure 11.** VLE-count deviation versus ‘remaining’-count deviation for all the dip events excluding event 7, 101 and 107, which have a ‘remaining’ deviation larger than 10. The dashed lines are discussed in the text.

Only event 4 and event 66 show obvious asymmetry in their light curve, that is, with fast drop and slow recovery in the flux. We suggest that, in the context of the above discussion, the 12 events, whose light curves are plotted in Fig. 12, are

probable non-instrumental events. It is about 10% of all the identified dip events.



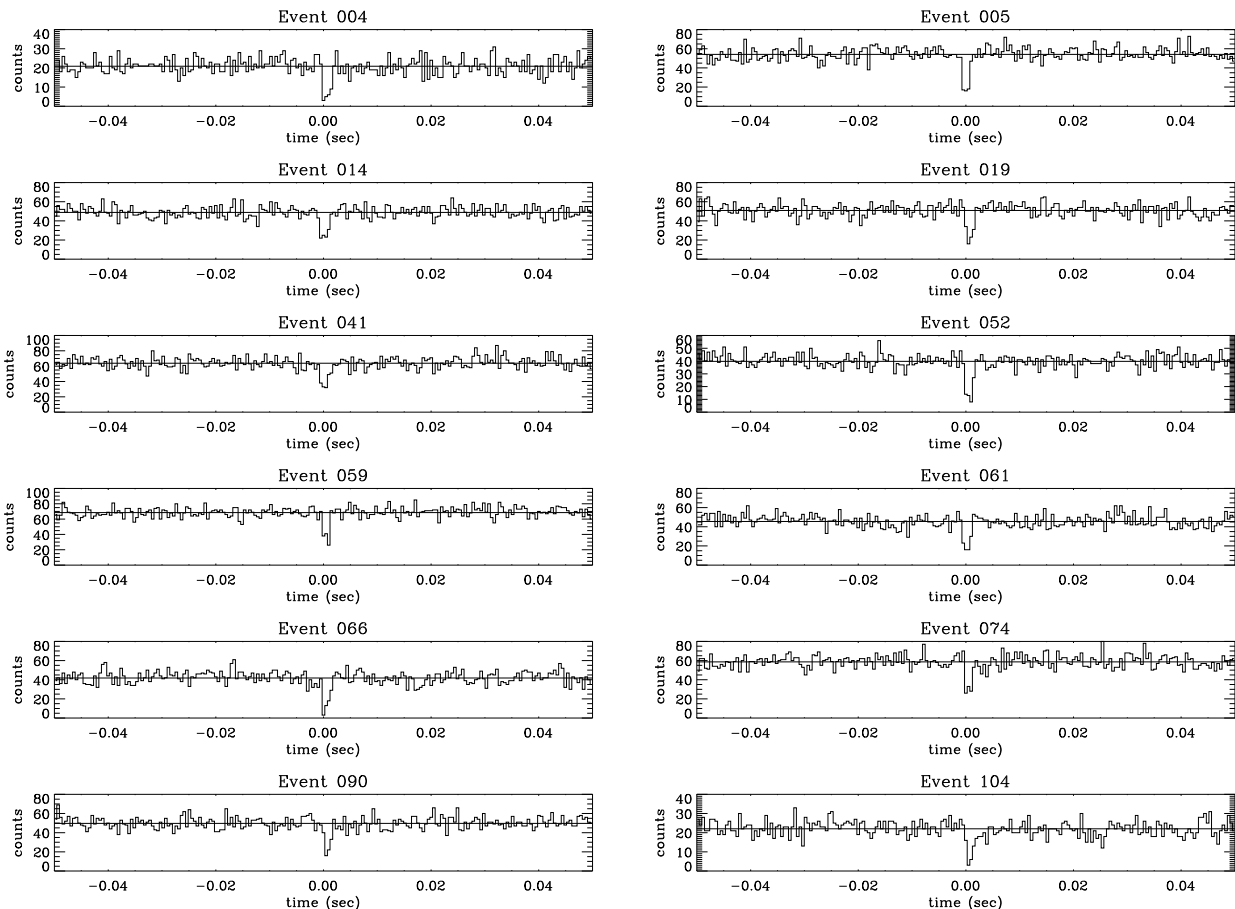


Figure 12. Light curves of the 12 proposed probable non-instrumental events.

## 5 TNO OCCULTATION AND SIZE DISTRIBUTION

Hereafter we assume the 12 probable events proposed above are really non-instrumental. These events of abrupt and significant flux drop at millisecond time scales are not random fluctuations, as evidently shown in the deviation distribution (e.g. Fig. 1). Based on spectral analysis, X-ray emission from *Sco X-1* is believed to originate from the neutron star surface thermal emission and corona comptonization near the inner accretion disk (e.g. Bradshaw, Geldzahler & Fomalont (2003); Barnard, Church & Balucinska-Church (2003)). A sudden quench of X-ray emission from *Sco X-1* in such a short time scale seems very unlikely. We have also examined the X-ray color for those events with two spectral channels. No detectable color change in the X-ray emission before and after any event was found. Occultation by objects in the line of sight is the most viable cause for these events.

The flux-drop fraction,  $A$ , of these events ranges from 0.36 to 0.72. To have such a significant flux drop, the occulting body must be a few times larger than the corresponding Fresnel scale, which is  $\sqrt{\lambda d/2}$ , where  $\lambda$  is the wavelength and  $d$  is the distance. It is about 30 m for  $d = 40$  AU and  $\lambda = 0.3$  nm (4 keV; most photons in the data are at this energy). Some X-ray diffraction patterns for objects of different sizes at different distances are computed and plotted in Fig. 13, with the PCA-detected photon spectrum from

*Sco X-1* as the input radiation for the computation. Fig. 13 shows the case for a spherical blocking object and a crossing impact parameter equal to 0.33. The crossing impact parameter is the distance to the shadow center in units of the object size. Computations with different crossing impact parameters, such as 0 and 0.67, do not yield too different a flux-drop fraction, although the diffraction patterns are different, particularly regarding the central brightening in the shadow. From the diffraction pattern computation, one can see that to have  $A \approx 0.3$ , the size of the occulting body at 40 AU away must be larger than 30 m, the Fresnel scale of 4-keV photons. We note that, given a certain ratio of the object size to the square root of the distance, the diffraction patterns are the same, up to a scaling factor in length proportional to the object size or the square root of the distance (e.g. Roques, Moncuquet & Sicardy (1987)). The flux-drop fraction  $A$  is therefore also the same for these patterns. At the distance of *Sco X-1*, 2.8 kpc (Bradshaw, Fomalont & Geldzahler 1999), the Fresnel scale is about 100 km (hereafter all the Fresnel scales are referred to that for 4-keV photons). It is clear if these events are occultation by objects moving around *Sco X-1*, those objects must be larger than about 100 km and also larger than the X-ray emitting region, which ranges from a few hundred kilometers to about 50,000 km, depending on different models (e.g. Bradshaw, Geldzahler & Fomalont (2003); Barnard, Church & Balucinska-Church (2003)). To produce

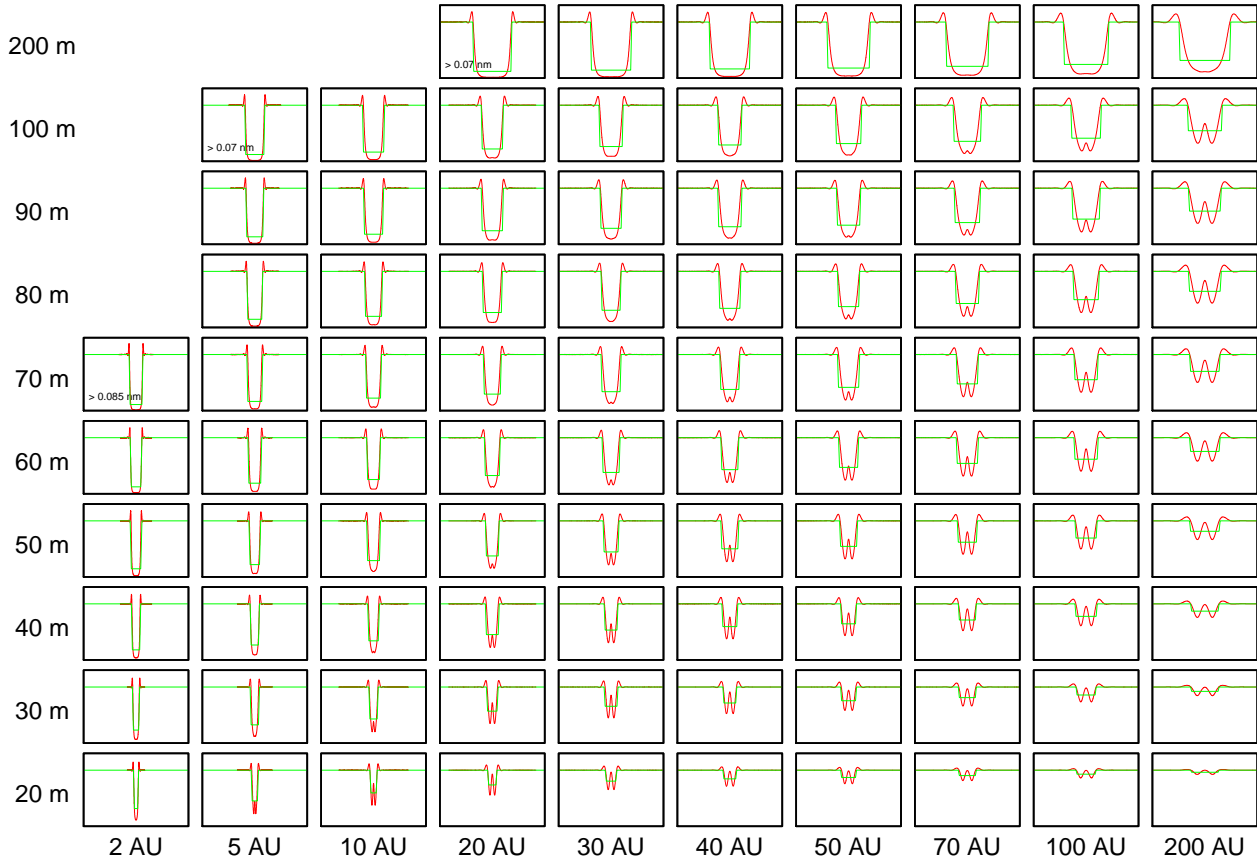


**Figure 13.** X-ray diffraction patterns (one-dimensional cut through a shadow) for objects of different sizes at different distances. The X-ray spectrum considered here is that of the RXTE/PCA observed photons from the Sco X-1, roughly in the energy range from 2 keV to 20 keV and peaked at about 4 keV. The effect of the varying spectrum of Sco X-1 on these patterns is negligible. The occulting object is assumed to be spherical. The patterns shown here assume a crossing impact parameter of 0.33, which is the distance from the shadow center in units of the object size. The width of each panel is 600 m. An equivalent square function pattern is also plotted in each panel, whose depth is the flux-drop fraction  $A$  discussed in the text. One can see that to have a flux-drop fraction of 0.3, the object is about the corresponding Fresnel scale of 4-keV photons. Note that the width of the square function here is wider than the corresponding duration of the dip events as we define in this paper.

a 2-ms event, the speed of those objects needs to be larger than  $5 \times 10^4$  km/sec, a very unlikely speed. If we consider, more realistically, the event duration as the shadow size instead of the object size, an even higher speed is required. The same argument can be applied to other objects in the interstellar space.

For objects at the distance of the Oort Cloud, typically 10,000 AU, the Fresnel scale is about 500 m. Again, to produce the events that we found, the Oort Cloud objects need to be larger than that scale. It is unlikely that a kilometer-size object in the Oort Cloud can produce millisecond events, since its speed relative to the earth is only about 30 km/sec. On the other hand, other solar system small bodies at a shorter distance can satisfy the duration and flux-drop constraints at the same time. A major source candidate is the main-belt asteroids. Their expected event rate for occulting Sco X-1, however, is too low ( $10^{-9}$  sec $^{-1}$ , down to 10-m size; see Chang et al. (2006)). We therefore propose that the 12 events, if really not instrumental, are occultation caused by objects in the trans-Neptunian region, that is, by TNOs.

To pin down the distance and the size of each occulting

body more accurately for all the events is an important issue but requires further analysis on the dead-time-corrected light curves, diffraction patterns and different orbital inclinations and eccentricities. That study will be reported in another forthcoming paper. For an approximate estimation of the occulting-object sizes at this stage, we contend ourselves by considering a typical relative speed of 30 km/s between the occulting TNOs and RXTE and a random crossing through the shadow. The average crossing length of a random crossing is  $\frac{\pi}{4}$  times that of a central crossing, assuming a circular shadow. We therefore set the size range of these 12 objects to be from 60 m to 100 m for durations from 1.5 ms to 2.5 ms. We note that the orbital speed of the Earth is about 30 km/s, RXTE's speed relative to the Earth is about 7 km/s, a TNO at 43 AU has an orbital speed about 5 km/s for a low eccentricity orbit, the shadow size is larger than the object, and our definition of the event duration tends to somewhat underestimate.

We next proceed to estimate the total number of TNOs of these sizes. For a background point source, the event rate is

$$\frac{N}{T} = \frac{\int_{s_1}^{s_2} \left(\frac{dN}{ds}\right) sv ds}{d^2 \Omega_A} , \quad (2)$$

where  $N$  is the number of detected events (assuming a 100% detection efficiency),  $T$  the total exposure time,  $\left(\frac{dN}{ds}\right)$  the differential size distribution,  $v$  the typical sky-projection relative speed,  $d$  the typical distance to the TNOs, and  $\Omega_A$  the total solid angle of the sky distributed with TNOs. To derive  $\left(\frac{dN}{ds}\right)$  from the event rate, a functional form of the distribution needs to be assumed. On the other hand, if the integration is only over a small range of the size, we may derive an average value at that size. Noting that  $\frac{dN}{d \log s} = \frac{dN}{ds} s \ln 10$ , we have

$$\int_{s_1}^{s_2} \left(\frac{dN}{ds}\right) sv ds = \left(\frac{dN}{d \log s}\right)_{s_1 < s < s_2} \frac{v(s_2 - s_1)}{\ln 10} , \quad (3)$$

and

$$\left(\frac{dN}{d \log s}\right)_{s_1 < s < s_2} = \frac{d^2 \Omega_A}{v(s_2 - s_1)} \frac{N}{T} \ln 10 . \quad (4)$$

We can estimate  $\Omega_A$  with the inclination distribution obtained from the CFHT survey (Trujillo, Jewitt & Luu 2001), which reported a  $20^\circ$  half-angle of an assumed gaussian distribution. This half-angle in the inclination distribution translates to about  $12.8^\circ$  for a corresponding half-angle in the apparent ecliptic latitude distribution, assuming circular orbits. Sco X-1 is  $5.5^\circ$  north of the ecliptic. To use the detection rate in the direction toward Sco X-1 to represent the whole TNO population, the equivalent sky area is a zone occupying  $\pm 15.5^\circ$  in latitude. Therefore,  $\Omega_A = 360 \times 31 \times \left(\frac{\pi}{180}\right)^2 = 3.4$ . Assuming a typical distance  $d = 43$  AU, a typical relative sky-projection speed  $v = 30$  km/s, and  $T = 564.3$  ks, we have in the size range from 60 m to 100 m

$$\left(\frac{dN}{d \log s}\right) \approx 5.7 \times 10^{15} . \quad (5)$$

The total number of TNOs in that size range is about  $1.3 \times 10^{15}$ .

There are considerable uncertainties in the above estimate. First of all, the suggestion that 12 out of the 107 dip events are non-instrumental is inconclusive. The detection efficiency of the procedure that we employed needs to be investigated in more details. The size of these possible occulting TNOs is only very roughly estimated. With all these cautions in mind, we tentatively discuss the implication of the discovery of TNO X-ray occultations. The estimated total number, about one quadrillion, for TNOs of size between 60 m and 100 m is several orders of magnitude larger than usual model predictions, but is close to, within the  $1-\sigma$  level, the direct extrapolation of the distribution obtained from the CFHT survey (Trujillo, Jewitt & Luu 2001), which gives a best fit of  $dN/ds \propto s^{-q}$  with  $q = 4.0_{-0.5}^{+0.6}$  ( $1 \sigma$ ) and the total number for TNOs larger than 100 km equal to  $3.8_{-1.5}^{+2.0} \times 10^4$  (Fig. 14). Our result seems to indicate that the power-law size distribution of TNOs may extend down to the order of 100 m without any breaking or flattening. On the other hand, if the assumed albedo is appropriate when converting the luminosity function into a size distribution from the HST observation (Bernstein et al. 2004), and if that size distribution inferred from 3 detections in 0.02 square degrees of the sky is reliable, a break will occur at about 50 km and there

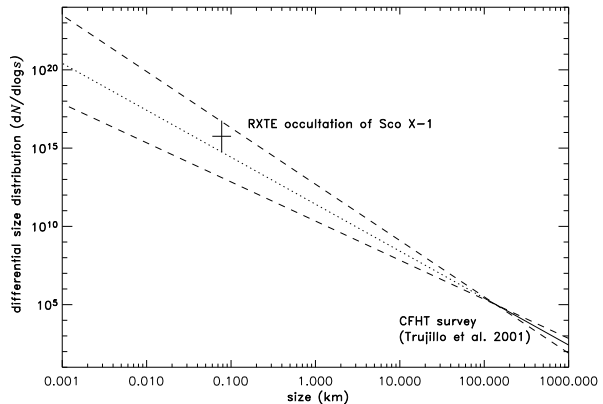


**Figure 14.** The differential size distribution of TNOs. The total number of TNOs per decade of size  $\left(\frac{dN}{d \log s}\right)$  inferred from the RXTE occultation of Sco X-1 is plotted as the cross with a symbolic uncertainty level of a factor of ten. The solid and dotted lines are the best fit from the CFHT survey (Trujillo, Jewitt & Luu 2001) and its extrapolation towards smaller sizes. The dashed lines mark its  $1-\sigma$  uncertainty in the power index of the distribution. Direct imaging of TNOs down to size of about 30 km were reportedly achieved by the Hubble Space Telescope (Bernstein et al. 2004), whose estimated TNO size distribution at about 30 km is a factor of 25 below the extrapolation of the afore mentioned CFHT survey. The Taiwanese-American Occultation Survey (TAOS) is expected to detect occultation events caused by TNOs of kilometre size (Alcock et al. 2003).

must exist a second component at smaller sizes. This second component may require a new mechanism in the theory of planet formation.

## 6 SUMMARY

We report 107 dip events of millisecond time scales in 564.3-ks RXTE/PCA archival data of Sco X-1. These dip events are apparently contaminated by those due to instrumental dead-time effects induced by high-energy cosmic rays. We performed detailed analysis and propose that about 10% of these dip events are probable TNO-occultation events. The inferred size distribution of TNOs at size about 100 m is several orders of magnitude larger than current theoretical predictions. Confirming or disproving this result is important for our understanding of planet formation processes in the early solar system. X-ray diffraction patterns in the occultation light curves may also be exploited to study the background X-ray source, potentially in a very high angular resolution. It is unfortunately impossible to definitely separate true occultation events from instrumental ones with currently available data. Observations of RXTE/PCA with an adequately designed data mode or of other new instruments in the future may resolve this issue.

## ACKNOWLEDGMENTS

We thank R. Rothschild, F. Roques, and G. Georgevits for helpful discussion. The examination of the event rate versus the time-since-SAA with the SAA passage determined

from HEXTE/PM data were first done by Tommy Thompson and Richard Rothschild. This research has made use of data obtained through the High Energy Astrophysics Science Archive Research Center Online Service, provided by the NASA/Goddard Space Flight Center, and of the JPL HORIZONS on-line solar system data and ephemeris computation service. This work was supported by the National Science Council of the Republic of China under grant NSC 95-2112-M-007-050 and by Academia Sinica in Taipei.

## REFERENCES

- Alcock C., Dave R., Giammarco J., Goldader J., Lehner M., King S.-K., Lee T., Wang A., Wang S.-Y., Wen C.-Y., et al., 2003, *Earth, Moon, and Planet*, 92, 459
- Bailey M.E., 1976, *Nature*, 259, 290
- Barnard R., Church M.J., Balucinska-Church M., 2003, *A&A*, 405, 237
- Bernstein G.M., Trilling D.E., Allen R.L., Brown M.E., Holman M., Malhotra R., 2004, *AJ*, 128, 1364
- Bradshaw C.F., Fomalont E.B., Geldzahler B.J., 1999, *ApJ*, 512, L121
- Bradshaw C.F., Geldzahler B.J., Fomalont E.B., 2003, *ApJ*, 592, 486
- Bradt H.V., Rothschild R.E., Swank J.H., 1993, *A&AS*, 97, 355
- Brown M.J.I., Webster R.L., 1997, *MNRAS*, 289, 783
- Chang H.-K., King S.-K., Liang J.-S., Wu P.-S., Lin L.C.-C., Chiu J.-L., 2006, *Nature*, 442, 660
- Cooray A., Farmer A.J., 2003, *ApJ*, 587, L125
- Edgeworth K.E., 1943, *J. Br. Astron. Soc.*, 53, 181
- Edgeworth K.E., 1949, *MNRAS*, 109, 600
- Farinella P., Davis D.R., Stern S.A., 2000, in *Protostars and Planets IV*, eds Mannings V., Boss A.P., Russel S.S. (The University of Arizona Press, Tucson), pp 1255-1282
- Jahoda K., et al., 2006, *ApJS*, 163, 401
- Jewitt D.C., Luu J.X., 1993, *Nature*, 362, 730
- Jones T.A., Levine A.M., Morgan E.H., Rappaport S., 2006, *astro-ph/0612129*
- Kenyon S.J., 2002, *PASP*, 114, 265
- Kenyon S.J., Bromley B.C., 2004, *AJ*, 128, 1916
- Kuiper G.P., 1951, in *Astrophysics*, ed Hynek J.A. (McGraw-Hill, New York), pp 357-424
- Leonard F.C., 1930, *Leaflet Astron. Soc. Pacific*, 80, 121
- Luu J.X., Jewitt D.C., 2002, *ARA&A*, 40, 63
- Oort J.H., 1950, *Bull. Astron. Inst. Netherlands*, 11, 91
- Press W.H., Teukolsky S.A., Vetterling W.T., Flannery B.P., 1992, *Numerical Recipes in C* (Cambridge University Press, Cambridge), pp 610-615.
- Roques F., Doressoundiram A., Dhillon V., Marsh T., Bickerton S., Kavelaars J.J., Moncuquet M., Auvergne M., Belskaya I., Chevreton M., et al., 2006, *AJ*, 132, 819
- Roques F., Moncuquet M., Lavilloni re N., Auvergne M., Chevreton M., Colas F., Lecacheux J., 2003, *ApJ*, 594, L63
- Roques F., Moncuquet M., Sicardy B., 1987, *AJ*, 93, 1549
- Rothschild R.E., et al., 1998, *ApJ*, 496, 538
- Trujillo C.A., Jewitt D.C., Luu J.X., 2001, *AJ*, 122, 457